

Complexes of Click-Derived Bistriazolylpyridines: Remarkable Electronic Influence of Remote Substituents on Thermodynamic Stability as well as Electronic and Magnetic Properties

Marc Ostermeier,^[a] Marie-Anne Berlin,^[a] Robert M. Meudtner,^[a] Serhiy Demeshko,^[b] Franc Meyer,^[b] Christian Limberg,^{*[a]} and Stefan Hecht^{*[a]}

Abstract: 2,6-Bis(1,2,3-triazol-4-yl)pyridine (btp) ligands with substitution patterns ranging from strongly electron-donating to strongly electron-accepting groups, readily prepared by means of Cu-catalyzed 1,3-dipolar cycloaddition (the “click” reaction), were investigated with regard to their complexation behavior, and the properties of the resulting transition-metal compounds were compared. Metal–btp complexes of 1:1 stoichiometry, that is, [Ru(btp)Cl₂(dmsO)] and [Zn(btp)Br₂], could be isolated and were crystallographically characterized: they display octahedral and trigonal-bipyramidal coordination geometries, respectively, and exhibit high aggregation tendencies due to efficient π – π stacking leading to low solubilities. Metal–btp complexes of 1:2 stoichiometry, that is, [Fe(btp)₂]²⁺ and [Ru(btp)₂]²⁺, could also be synthesized and their metal centers show the expected octahedral coordination spheres. The iron compounds

exhibit quite a complex magnetic behavior in the solid state including spin crossover near room temperature, and hysteresis and locking into high-spin states on tempering at 400 K, depending on the substituents on the btp ligands. Cyclic voltammetry studies of [Ru(btp)₂]²⁺ reveal strong modulation of the oxidation potentials by more than 0.6 V and a clear linear correlation to the Hammett constant (σ_{para}) of the substituent at the pyridine core. Isothermal titration calorimetry was used to measure the thermodynamics of the Fe^{II}–btp complexation process and enabled accurate determination of the complexation enthalpies, which display a linear relationship with the σ_{para} values for the terminal phenyl substitu-

ents. Detailed NMR spectroscopic studies finally revealed that in the case of Fe^{II} complexation, dynamics are rapid for all investigated btp derivatives in acetonitrile, while replacing Fe^{II} by Ru^{II} or changing the solvent to dichloromethane effectively slows down ligand exchange. The results nicely demonstrate the utility of substituent parameters, originally developed for linear free-energy relationships to explain reactivity in organic reactions, in coordination chemistry, and to illustrate the potential to custom-design btp ligands and complexes thereof with predictable properties. The fast equilibration of the [Fe(btp)₂]²⁺ complexes together with their tunable stability and interesting magnetic properties should enable the design of dynamic metallosupramolecular materials with advantageous properties.

Keywords: click chemistry • coordination chemistry • isothermal titration calorimetry • substituent effects • tridentate ligands

[a] Dipl.-Chem. M. Ostermeier, Dipl.-Chem. M.-A. Berlin, Dr. R. M. Meudtner, Prof. Dr. C. Limberg, Prof. Dr. S. Hecht
Department of Chemistry
Humboldt-Universität zu Berlin
Brook-Taylor-Strasse 2, 12489 Berlin (Germany)
Fax: (+49) 30-2093-6940
E-mail: christian.limberg@chemie.hu-berlin.de
sh@chemie.hu-berlin.de

[b] Dr. S. Demeshko, Prof. Dr. F. Meyer
Institut für Anorganische Chemie
Georg-August Universität
Tammannstrasse 4, 37073 Göttingen (Germany)

Supporting information (containing experimental details) for this article is available on the WWW under <http://dx.doi.org/10.1002/chem.201000721>.

Introduction

For a given metal ion the chemical and physical properties of its complexes are determined by the surrounding ligand environment. Consequently, the development of tailor-made ligands continues to be a very active field of research, since the design of novel ligands is the key to new and improved properties and applications. One ligand motif, which has been utilized extensively in the past, contains a central pyridine unit flanked by heteroaromatic residues, such as pyridyl (i.e., 2,2':6',2''-terpyridine (tpy)),^[1] oxazolanyl (i.e., bis(oxazolanyl)pyridine (pybox)),^[2] and pyrazolyl.^[3] These tridentate

ligands have enabled the design of various macromolecular and supramolecular architectures,^[1b] optoelectronic^[1b,4] and magnetic^[5] materials as well as enantioselective catalysts.^[6] However, variation of the ligand scaffolds proves cumbersome in many cases, and therefore the facile and modular synthesis of a broad range of representatives of the above-mentioned ligand families remains an important yet difficult task. To address this issue, we have recently applied click chemistry^[7,8] to synthesize 2,6-bis(1-aryl-1,2,3-triazol-4-yl)pyridine (btp)^[9] compounds as versatile extended heteroaromatic building blocks to exploit their conformational preferences in macromolecular and supramolecular chemistry^[10] and to utilize the btp ligand scaffold in coordination chemistry.^[9,11] A diverse set of symmetrical and nonsymmetrical btp molecules carrying electron-donating and -withdrawing substituents at both terminal aryl moieties and the central pyridine core has efficiently been synthesized, and in preliminary studies the complexation behavior of two representatives in the presence of Fe²⁺ and Eu³⁺ ions has been investigated. During the course of these initial studies one [Fe(btp)₂]²⁺ complex as well as one [Eu(btp)₃]³⁺ complex were prepared and could be characterized by single-crystal X-ray structure analysis. Whereas the latter Eu complex exhibited a characteristic luminescence in solution and in the solid state, the Fe complex surprisingly exhibited a low-spin configuration at room temperature, which illustrates that the field strength of the particular btp derivative is significantly higher than the one of bis(pyrazolyl)pyridine^[3] yet comparable to the field strength of tpy.^[12]

In view of these initial results, we were interested in a thorough analysis of the coordination chemistry of a diverse set of btp ligands (Figure 1). Here, we report on the complexation behavior of a wide range of btp derivatives in so-

lution and present the structures as well as the electronic and magnetic properties of the resulting complexes. In particular, we show that the complexation thermodynamics as well as the redox properties are strongly influenced by the ligand electronics and can be quantitatively correlated to classical substituent effects at the terminal aryl and central pyridine moieties, that is, R¹, R², and R³ shown in Figure 1.

Results and Discussion

The btp ligands: The employed btp ligands were prepared by using our recently described procedure^[9] through a two-fold click reaction of various terminal aryl azides possessing electronically different substituents ranging from strongly donating (–NMe₂) to strongly accepting (–NO₂), with several 2,6-diethynylpyridine cores, again possessing either donating or accepting substituents in their 4-position, that is, btp ligand series **1a–d** and **2a–c**, respectively.^[9] Complementary to our previous work, three additional btp ligands possessing no central triethylene glycol chains (Tg), that is, btp ligands **3a–c**, were prepared^[13] to facilitate crystallization and structural refinement of the derived metal complexes. Due to the strong conformational preference of the btp scaffold to adopt the *anti,anti* conformation, all free ligands crystallize in a horseshoe-like kinked structure (see Figures 5–7 in the Supporting Information).

Metal–btp complexes with a metal-to-ligand ratio of 1:1:

The metal centers of the complexes reported so far with btp ligands of the type shown in Figure 1 are coordinatively saturated by btp ligands exclusively^[9] or by a combination of btp and tpy.^[11c] Hence, no free coordination sites are available to, for instance, coordinate other ligands for structural modifications or to bind substrates for activation during the course of catalysis; note that, for instance, complexes of bis(imino)pyridines, which may be considered as a related ligand class, with a metal-to-ligand ratio of 1:1 proved efficient catalysts for polymerization/oligomerization reactions.^[14] We were therefore also interested in metal–btp complexes with more asymmetric coordination spheres. As Ru^{II} in combination with polydentate N-heteroaromatic ligands, in particular tpy derivatives, can lead to advantageous optoelectronic phenomena exploited in light-harvesting applications,^[4,15] we set out to investigate the synthesis of Ru^{II}–btp complexes. Starting from the common precursor [RuCl₂(dmsO)₄]^[16] dissolved in acetonitrile, addition of ligand **1a** or **1b** leads to a color change from yellow to orange within 30 min and the orange-colored complexes [Ru(**1b**)Cl₂(dmsO)] and [Ru(**1a**)Cl₂(dmsO)], respectively, slowly start to precipitate. The conversion can be accelerated by heating the reaction mixture at reflux, from which the formed complexes then precipitate within a few hours. Importantly, solely 1:1 complexes were obtained by this procedure, independently of the molar ratio between the metal precursor and the btp ligand employed. In the case of btp ligands carrying no triethylene glycol units, that is, **3a–c**, problems with

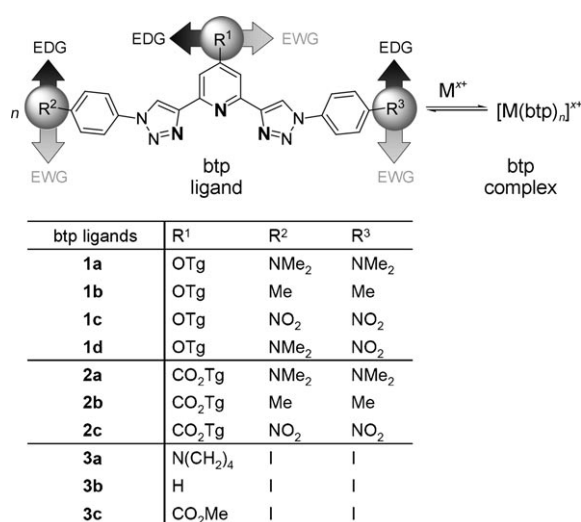


Figure 1. Tuning the electronics of tridentate 2,6-bis(1-aryl-1,2,3-triazol-4-yl)pyridine (btp) ligands (coordinating N atoms shown in bold) by varying R¹, R², R³ (gray circles) from electron-donating groups (EDG) to electron-withdrawing groups (EWG) to control metal coordination and complex properties (the free ligand is shown in the energetically less favorable *syn,syn* conformation); Tg = (CH₂CH₂O)₃CH₃.

their markedly lower solubilities in acetonitrile can be circumvented by the use of dichloromethane as the solvent, which allows for quantitative complex formation within 24 h of reflux. After filtration, washing with diethyl ether or dichloromethane, respectively, gave the orange-red complexes in very good yields and in analytically pure form, as evidenced by elemental analysis, ESI-MS, and NMR spectroscopy. However, single crystals could only be obtained in the case of $[\text{Ru}(\mathbf{3c})\text{Cl}_2(\text{dms})]$: Careful layering of solutions of $\mathbf{3c}$ and $[\text{RuCl}_2(\text{dms})_4]$ in dichloromethane with a minimum of diffusion occurring during this process allowed for in situ complex formation and crystal growth at the interface. This procedure led to cocrystallization of $[\text{Ru}(\mathbf{3c})\text{Cl}_2(\text{dms})]$ (Figure 2) and $\mathbf{3c}$ as revealed by X-ray diffraction.

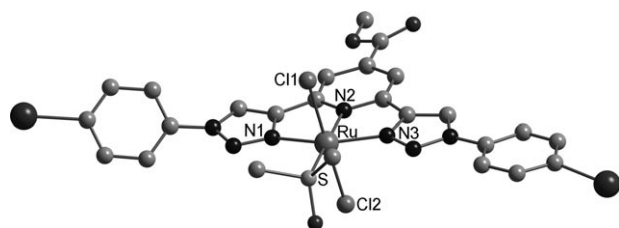


Figure 2. Molecular structure of $[\text{Ru}(\mathbf{3c})\text{Cl}_2(\text{dms})]$ (hydrogen atoms and a cocrystallized molecule of $\mathbf{3c}$ have been omitted for clarity).^[17] Selected bond lengths [Å] and angles [°]: Ru–N1 2.077(7), Ru–N2 2.015(9), Ru–N3 2.044(8), Ru–Cl1 2.428(2), Ru–Cl2 2.399(2), Ru–S 2.275(3); N1–Ru–N2 78.6(3), N1–Ru–N3 156.8(3), N1–Ru–Cl1 86.6(2), N1–Ru–Cl2 93.7(2), N1–Ru–S 103.1(3), N2–Ru–N3 78.2(4), N2–Ru–Cl1 90.4(3), N2–Ru–Cl2 89.2(3), N2–Ru–S 178.0(3), N3–Ru–Cl1 93.8(3), N3–Ru–Cl2 85.7(3), N3–Ru–S 100.2(3), Cl1–Ru–Cl2 179.44(8), Cl1–Ru–S 88.59(9), Cl2–Ru–S 91.79(9).

As expected, the btp ligand binds in a tridentate meridional mode at the ruthenium center, the coordination sphere of which is completed by two chlorido ligands and one dms molecule interacting through its S atom. Hence, a distorted octahedral geometry results and the main deviation from an ideal structure is caused by the positioning of the N atoms of the triazole rings: The N1–Ru–N3 angle amounts to 156.8° and is therefore much smaller than the ideal 180° of an undistorted octahedron. The remaining X–Ru–X' angles with X and X' oriented in *trans* positions (N2–Ru–S 178.0° , Cl1–Ru–Cl2 179.4°) are very close to 180° . The overall structural parameters of the complex are astonishingly similar to the respective tpy complex, that is, $[\text{RuCl}_2(\text{dms})(\text{tpy})]$.^[18]

To investigate whether the utilization of metal halides instead of triflates (that had led to 1:2 complexes)^[9] represents a more general approach to 1:1 metal–btp complexes, a solution of ZnBr_2 in acetonitrile was treated with a solution of btp ligand $\mathbf{1a}$ in acetonitrile. This immediately led to the precipitation of $[\text{Zn}(\mathbf{1a})\text{Br}_2]$ in the form of a white powder. Due to the poor solubility of the compound in common organic solvents, attempts to grow crystals were again performed by careful addition of a solution of the metal precursor

(ZnBr_2) in acetonitrile to a solution of the ligand ($\mathbf{1a}$) in acetonitrile. This procedure led to cocrystallization of $[\text{Zn}(\mathbf{1a})\text{Br}_2]$ (Figure 3) and ZnBr_2 .

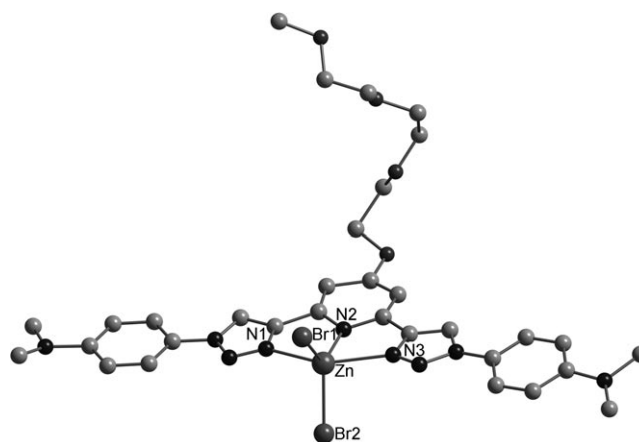


Figure 3. Molecular structure of $[\text{Zn}(\mathbf{1a})\text{Br}_2]$ (hydrogen atoms and cocrystallized ZnBr_2 and CH_3CN solvent molecules have been omitted for clarity).^[17] Selected bond lengths [Å] and angles [°]: Zn–N1 2.27(3), Zn–N2 2.10(2), Zn–N3 2.31(2), Zn–Br1 2.377(6), Zn–Br2 2.388(6); N1–Zn–N2 74.8(9), N1–Zn–N3 149.8(8), N1–Zn–Br1 96.2(7), N1–Zn–Br2 94.5(6), N2–Zn–N3 75.1(8), N2–Zn–Br1 123.4(6), N2–Zn–Br2 110.5(6), N3–Zn–Br1 99.0(5), N3–Zn–Br2 97.3(6), Br1–Zn–Br2 126.0(2).

As envisaged, again only one btp ligand coordinates to the zinc center, which additionally binds two bromido ligands, such that the coordination sphere of the Zn ion can be described as distorted square pyramidal ($\tau^{[19]}=0.46$). Whereas the overall structure resembles the analogous $[\text{ZnCl}_2(\text{tpy})]$ complex^[20] and the central Zn–pyridine bond lengths in both complexes are comparable, the bonds of the terminal triazole N atoms to the Zn center are more than 0.1 \AA longer than the 2-pyridyl–Zn bonds in the tpy complex ($2.185(3) \text{ \AA}$).

The observed very low solubilities in common organic solvents, enabling the facile isolation of the 1:1 metal–btp complexes, appear to originate from extensive π – π stacking interactions^[21] between the btp entities leading to a layered arrangement in the crystalline solid (Figure 4). The distances between the individual yet not exactly parallel planes of the metal–btp frameworks amount to 3.3 – 3.7 \AA in $[\text{Zn}(\mathbf{1a})\text{Br}_2]$ and to only 3.1 – 3.3 \AA in $[\text{Ru}(\mathbf{3a})\text{Cl}_2(\text{dms})]$, respectively. The layered arrangement is additionally supported by hydrogen bonds between the MX_2 moieties and C–H units of triazole and pyridine rings belonging to adjacent molecules.^[22]

Metal–btp complexes with a metal-to-ligand ratio of 1:2

Synthesis and structure: The published syntheses for $[\text{RuL}_2]^{2+}$ (with $\text{L} = \text{tpy}$ ^[18b,23] or a more simple representative of the btp ligand family with alkyl groups at the triazole units^[11a]) commonly exploit $[\text{RuCl}_2(\text{dms})_4]$ ^[16] as the Ru source in combination with NH_4PF_6 dissolved in high-boiling

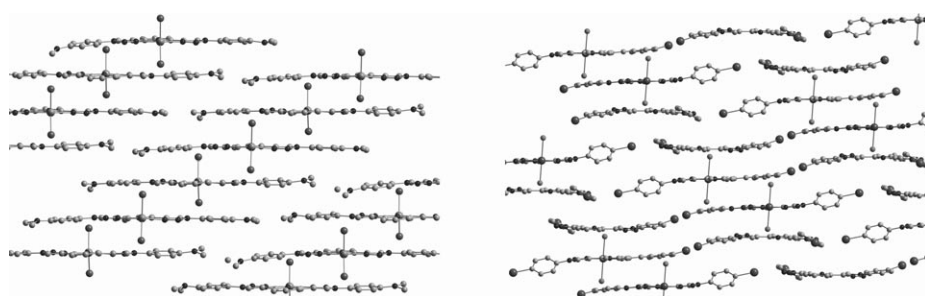


Figure 4. Packing diagram of $[\text{Zn}(\mathbf{1a})\text{Br}_2]$ (left; OTg groups, hydrogen atoms, cocrystallized ZnBr_2 , and CH_3CN are omitted for clarity) and $[\text{Ru}(\mathbf{3c})\text{Cl}_2(\text{dms})]$ (right; cocrystallized ligand $\mathbf{3c}$ shown; COOMe groups, dms ligands, and hydrogen atoms are omitted for clarity).

solvents. We found that our route developed for the preparation of 1:1 Ru–btp complexes (vide supra) can also be utilized for the synthesis of 1:2 complexes when it is pursued in the presence of AgOTf (OTf = trifluoromethanesulfonate), which removes the more strongly bound chlorido ligands from the coordination sphere of the Ru center.^[24] Thus, treatment of $[\text{RuCl}_2(\text{dms})_4]$ with $\mathbf{1b}$ (2 equiv) and AgOTf (2 equiv) yielded the complex $[\text{Ru}(\mathbf{1b})_2](\text{OTf})_2$, which is highly soluble in DMF and therefore (in contrast to the 1:1 complexes) remains in solution, thereby facilitating separation from the AgCl precipitate. Isolation gave $[\text{Ru}(\mathbf{1b})_2](\text{OTf})_2$ as a yellow solid, which shows good solubility in acetonitrile and was fully characterized, yet no single crystals could be obtained.

By utilizing ligand $\mathbf{3b}$, which lacks the solubilizing triethylene glycol chain, $[\text{Ru}(\mathbf{3b})_2](\text{PF}_6)_2$ could be synthesized by heating $[\text{RuCl}_2(\text{dms})_4]$ and $\mathbf{3b}$ (2 equiv) in ethylene glycol at reflux followed by the addition of an aqueous solution of NH_4PF_6 . In a similar fashion complexes $[\text{Ru}(\text{btp})_2](\text{PF}_6)_2$ with $\text{btp} = \mathbf{3a}$, $\mathbf{3c}$, and $\mathbf{1b}$ were prepared, and for all of these compounds single crystals suitable for X-ray diffraction could be grown. Exemplarily, the molecular structure of $[\text{Ru}(\mathbf{3b})_2](\text{PF}_6)_2$ is shown in Figure 5; the other structures are depicted in Figures 10–13 in the Supporting Information. They are all very similar and resemble the structures previously found for $[\text{M}(\text{btp})_2]^{2+}$ ($\text{M} = \text{Ru}, \text{Fe}$).^[9,11a] The Ru center is coordinated by two $\mathbf{3b}$ ligands in a distorted-octahedral fashion, and the distances between the Ru center and the N atoms of the triazole rings are slightly longer than those involving the N atoms of the pyridine rings. In general, the 1:2 complexes—unlike the 1:1 complexes (vide supra)—are readily soluble in polar organic solvents, such as acetonitrile and benzonitrile, as neither a layered structure with π – π interactions nor a network of hydrogen bonds can be formed.

The selective formation of 1:1 complexes (even under forcing conditions or in the presence of an excess amount of btp) on the one hand, and the possibility to introduce a second btp ligand at the Ru center (through the addition of AgOTf or heating followed by the addition of NH_4PF_6) on the other hand, can be utilized for the preparation of complexes containing two different btp ligands. This is exemplified by the synthesis of complex $[\text{Ru}(\mathbf{1a})(\mathbf{1b})](\text{PF}_6)_2$ through

treatment of $[\text{Ru}(\mathbf{1b})\text{Cl}_2(\text{dms})]$ with $\mathbf{1a}$ in the presence of NH_4PF_6 . $[\text{Ru}(\mathbf{1a})(\mathbf{1b})](\text{PF}_6)_2$ could be isolated as a lemon-colored solid and $^1\text{H NMR}$ spectroscopy as well as ESI-MS measurements^[13] clearly showed that two different ligands are bound to each of the Ru centers, thus excluding a 1:1 mixture of the corresponding homoleptic complexes.

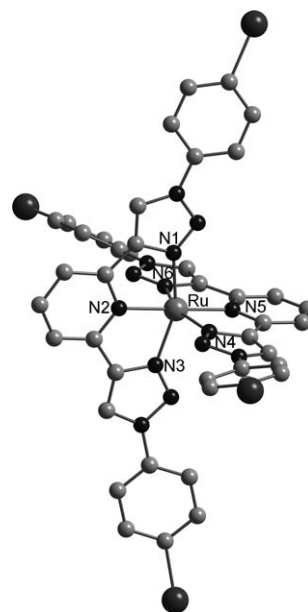


Figure 5. Molecular structure of $[\text{Ru}(\mathbf{3b})_2](\text{PF}_6)_2$ (hydrogen atoms, PF_6 anions, and cocrystallized solvent molecules have been omitted for clarity).^[17] Selected bond lengths [Å] and angles [°]: Ru–N1 2.066(9), Ru–N2 2.023(7), Ru–N3 2.056(9), Ru–N4 2.045(8), Ru–N5 2.031(7), Ru–N6 2.046(8); N1–Ru–N2 78.6(3), N1–Ru–N3 157.0(3), N1–Ru–N4 92.7(3), N1–Ru–N5 101.6(3), N1–Ru–N6 91.7(3), N2–Ru–N3 78.5(3), N2–Ru–N4 104.0(3), N2–Ru–N5 178.2(3), N2–Ru–N6 98.9(3), N3–Ru–N4 92.1(3), N3–Ru–N5 101.3(3), N3–Ru–N6 92.6(3), N4–Ru–N5 77.8(3), N4–Ru–N6 157.1(3), N5–Ru–N6 79.3(3).

An important aspect of the btp coordination chemistry is related to the question of how the substituents on the aryl rings of the terminal triazole units and those on the central pyridyl entity influence the coordination behavior of the ligands and thus the properties of the resulting complexes. If significant substituent effects are unraveled, facile tuning of the ligand framework could be achieved. In the following sections, we discuss this possibility to electronically modulate the btp framework.

Magnetic properties: A first indication for the relevance of this aspect came from a closer inspection of the magnetic behavior of $[\text{Fe}(\mathbf{1c})_2](\text{OTf})_2$, for which a low-spin \rightarrow high-spin transition was expected to occur at elevated tempera-

tures.^[9] Indeed, when $[\text{Fe}(\mathbf{1c})_2](\text{OTf})_2$ was heated to 200 °C the red-brown powder changed its color to yellow. Surprisingly, the original red-brown color could not be re-established by cooling and not even by storage at –30 °C for several weeks or at –196 °C for several days. It could be regenerated, though, by dissolving the complex in acetonitrile at room temperature. Whereas in solution thermally induced spin transitions proceed gradually, in the solid state their devolution can vary quite significantly, depending on whether long-range cooperative effects become operative.^[25] For a closer inspection of the spin transition at higher temperatures we measured $\chi_M T$ (χ_M = molar magnetic susceptibility) at a magnetic field of 5000 Oe in the temperature range 5–400 K (Figure 6).

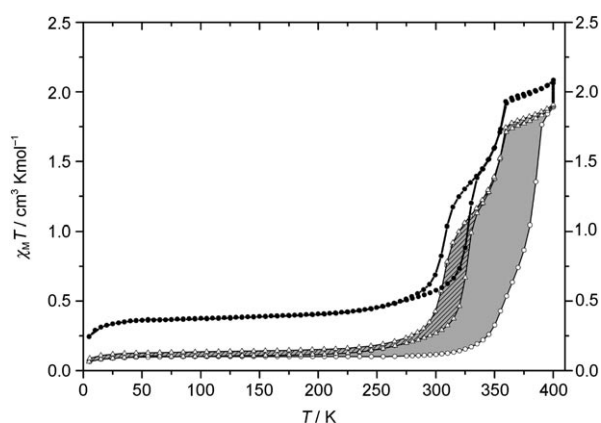


Figure 6. Temperature dependence of $\chi_M T$ for $[\text{Fe}(\mathbf{1c})_2](\text{OTf})_2$ (temperature-independent paramagnetism, $\text{TIP} = 1795 \times 10^{-6} \text{ cm}^3 \text{ mol}^{-1}$ is subtracted). Progress of T program: \circ = 1st hysteresis loop: 5–400–5 K, gray area; \triangle = 2nd hysteresis loop: 5–400–5 K, dashed area; \bullet = 1 h at 400 K; \bullet = 3rd hysteresis loop: 400–5–400 K, white area.

Starting from low-spin $[\text{Fe}(\mathbf{1c})_2](\text{OTf})_2$ held at 5 K, raising the temperature has nearly no effect on $\chi_M T$ until reaching 325 K when $\chi_M T$ increases sharply, reaching a value of $1.90 \text{ cm}^3 \text{ K mol}^{-1}$ at 400 K. Recooling of the sample leads to a sharp decrease of the magnetic moment that parallels the increase on heating, but with a hysteresis at a 25–50 K lower temperature, and this process proved to be partially reversible in a further heating–cooling cycle (Figure 6). The low-temperature plateau of approximately $0.1 \text{ cm}^3 \text{ K mol}^{-1}$ might indicate the trapping of part of the sample (about 3%) in the high-spin state, possibly already in the course of the work-up procedure,^[13] and the fact that tempering (vide infra) increases the value of this plateau seems to support this. Dislocations and defects in the lattice are usually held responsible for such behavior in the case of a crystalline material.^[25]

To complement these findings, Mössbauer spectra of powdered $[\text{Fe}(\mathbf{1c})_2](\text{OTf})_2$ were recorded at 7, 80, 200, and 295 K. The spectrum at 80 K shows one doublet with $\delta = 0.36 \text{ mm s}^{-1}$ and $\Delta E_0 = 0.96 \text{ mm s}^{-1}$ (Figure 7a), and increasing the temperature to 295 K did not lead to basic changes

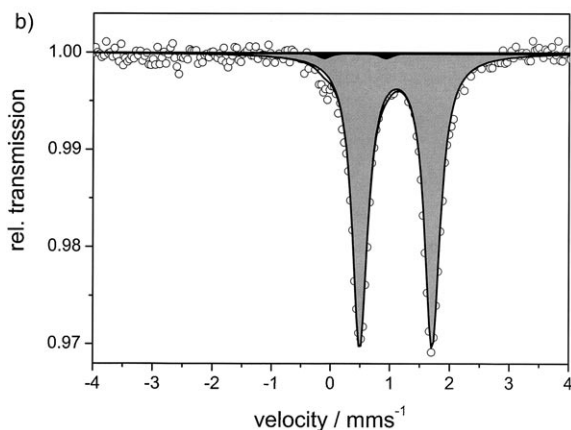
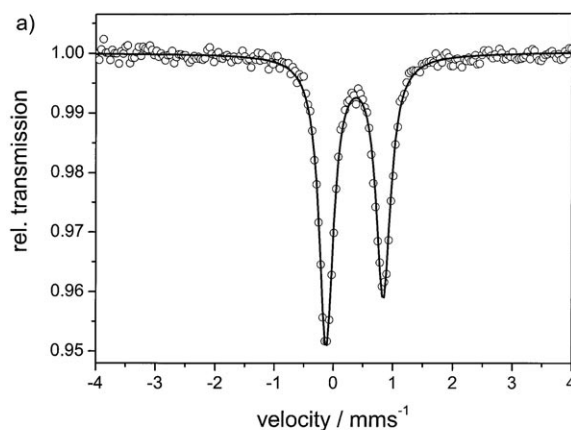


Figure 7. Mössbauer spectra of $[\text{Fe}(\mathbf{1c})_2](\text{OTf})_2$ measured at 80 K. a) “red” low-spin $[\text{Fe}(\mathbf{1c})_2](\text{OTf})_2$: $\delta = 0.36 \text{ mm s}^{-1}$ and $\Delta E_0 = 0.96 \text{ mm s}^{-1}$. b) “yellow” high-spin $[\text{Fe}(\mathbf{1c})_2](\text{OTf})_2$ resulting from heating of the red sample (a) to 200 °C for 30 min.

(Figures 21–24 in the Supporting Information). Its δ and ΔE_0 values are similar to those obtained for octahedral iron(II) low-spin complexes, such as $[\text{Fe}(\mathbf{3-bpp})_2](\text{OTf})_2 \cdot \text{H}_2\text{O}$ ^[26] ($\mathbf{3-bpp}$ = 2,6-bis(pyrazolyl-3-yl)pyridine; $\delta = 0.29 \text{ mm s}^{-1}$, $\Delta E_0 = 0.69 \text{ mm s}^{-1}$ at 140 K) or $[\text{Fe}(\mathbf{1-bpp})_2](\text{BF}_4)_2$ ^[27c] ($\mathbf{1-bpp}$ = 2,6-bis(pyrazolyl-1-yl)pyridine; $\delta = 0.39 \text{ mm s}^{-1}$, $\Delta E_0 = 0.75 \text{ mm s}^{-1}$ at 80 K), and the results thus support the predominance of the low-spin state within the temperature range of 7–295 K.^[28]

The preliminary qualitative observations outlined above seemed to suggest that warming of $[\text{Fe}(\mathbf{1c})_2](\text{OTf})_2$ to higher temperatures (200 °C) causes irreversibility of the spin transition. Indeed, a magnetic measurement for a corresponding “yellow sample” showed a typical high-spin behavior with $\chi_M T$ varying only between 3.5 and $3.7 \text{ cm}^3 \text{ K mol}^{-1}$ in the temperature range 50–400 K (Figure 33 in the Supporting Information). Consistently, a high-spin doublet dominates the Mössbauer spectrum of such a sample (Figure 7b, gray area: $\delta = 1.10 \text{ mm s}^{-1}$ and $\Delta E_0 = 1.21 \text{ mm s}^{-1}$), while the intensity of the original low-spin signal decreased to only 1.7% (Figure 7b, black area: $\delta = 0.40 \text{ mm s}^{-1}$ and $\Delta E_0 = 1.04 \text{ mm s}^{-1}$).

To test whether tempering at temperatures somewhat lower than 200 °C (473 K) has a similar effect, $[\text{Fe}(\mathbf{1c})_2](\text{OTf})_2$ (which had experienced two heating–cooling cycles already) was kept at 400 K for one hour and its magnetic behavior was investigated during this time (Figure 6): $\chi_{\text{M}}T$ increased from 1.92 to 2.05 $\text{cm}^3\text{K mol}^{-1}$, and on cooling it decreased only to 0.62 $\text{cm}^3\text{K mol}^{-1}$ at room temperature (0.33 $\text{cm}^3\text{K mol}^{-1}$ before heating) and to 0.24 $\text{cm}^3\text{K mol}^{-1}$ at 5 K (0.07 $\text{cm}^3\text{K mol}^{-1}$ before heating). Consistently, a Mössbauer spectrum recorded subsequently at 80 K now showed beside the low-spin doublet (Figure 7a) a high-spin doublet as depicted in Figure 7b with a partitioning of 9% (Figure 25 in the Supporting Information). Hence, tempering at 400 K or—more rigorously—short periods of heating to 473 K (200 °C) antagonize the reversibility of the low-spin \leftrightarrow high-spin transition. A possible reason for this is the occurrence of structural rearrangements occurring at higher temperatures that favor elongated Fe–N bonds, characteristic for high-spin complexes. Variable-temperature X-ray analysis and powder X-ray diffraction were not possible. To further investigate this phenomenon differential scanning calorimetry (DSC) measurements were performed for the temperature range 250–475 K (Figure 20 in the Supporting Information), the results of which nicely complemented the magnetic measurements, and they can be summarized as follows: 1) on heating from 217 to 400 K a broad endothermic peak at 330 K with a shoulder at 360 K appears, which can be assigned to a two-stage low-spin \rightarrow high-spin transition, as well as a small additional peak that corresponds to a phase transition; 2) the phase transition at 390 K activates cooperativity during the spin crossover, as confirmed by a further magnetic measurement: If heating of the sample is stopped at 375 K, in corresponding cooling–heating cycles $\chi_{\text{M}}T$ decreases and increases only slowly; once a sample has been heated to 400 K, however, the spin crossover occurs far more abruptly, cooperatively, and reversibly (compare Figures 20 and 30 in the Supporting Information); 3) on heating of the sample to 473 K a third peak is observed at 430 K, whereby the residual low-spin molecules are transferred into the high-spin state, and hence the spin crossover proceeds in three steps. Having passed the third step, the crossover to the high-spin state becomes irreversible: on recooling to 224 K no features are observed anymore. Please note that heating does not lead to appreciable decomposition of $[\text{Fe}(\mathbf{1c})_2](\text{OTf})_2$ as shown by thermogravimetric analysis (Figure 19 in the Supporting Information).

Importantly, the partitioning of the high-spin state in a solid sample and also the conditions required to completely lock $[\text{Fe}(\text{btp})_2]^{2+}$ complexes into the high-spin state are dependent on the substituents on the aryl rings. Whereas the complex obtained from ligand **1c**, carrying electron-accepting NO_2 groups, has a $\chi_{\text{M}}T$ value of 0.1 $\text{cm}^3\text{K mol}^{-1}$ (compare Figure 6) at room temperature, it amounts to 3.5 $\text{cm}^3\text{K mol}^{-1}$ in the case of $[\text{Fe}(\mathbf{1b})_2](\text{OTf})_2$ (Figure 36 in the Supporting Information), which differs from $[\text{Fe}(\mathbf{1c})_2](\text{OTf})_2$ only by the replacement of the NO_2 groups by methyl substituents. Clearly the high-spin/low-spin ratio is

far higher in the latter case of the more electron-donating btp ligand and a quantitative analysis indicates a low-spin contribution of only 11.3% (Figure 37 in the Supporting Information). This is in agreement with the results of Mössbauer measurements performed for powdered samples of $[\text{Fe}(\mathbf{1b})_2](\text{OTf})_2$ at 7 and 80 K, which reveal a spin distribution of 90% high spin and 10% low spin (Figures 27 and 28 in the Supporting Information). Furthermore, whereas in the case of $[\text{Fe}(\mathbf{1c})_2](\text{OTf})_2$ initial heating cycles are reversible, display a hysteresis, and become irreversible only after prolonged heating, the corresponding complex incorporating methyl-substituted ligand **1b** remains quantitatively in the high-spin state once it has reached 400 K (Figures 36 and 37 in the Supporting Information). Finally, complex $[\text{Fe}(\mathbf{3a})_2](\text{OTf})_2$, composed of even more electron-donating btp ligands, was investigated with the expectation of an even more dominating high-spin state.

Notably, a $\chi_{\text{M}}T$ value of only 1.8 $\text{cm}^3\text{K mol}^{-1}$ was determined at room temperature, and besides this, the study of the temperature-dependent behavior of $[\text{Fe}(\mathbf{3a})_2](\text{OTf})_2$ revealed several astonishing effects (Figure 8): While initial

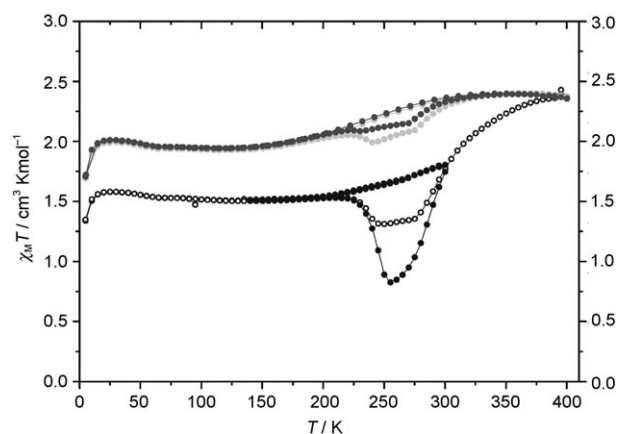


Figure 8. Temperature dependence of $\chi_{\text{M}}T$ for $[\text{Fe}(\mathbf{3a})_2](\text{OTf})_2$ (TIP = $1609 \times 10^{-6} \text{ cm}^3 \text{ mol}^{-1}$ is subtracted). Progress of T program: ● = 1st hysteresis loop: 300–140–300 K; ○ = 2nd hysteresis loop: 300–5–400 K; ● = 3rd hysteresis loop: 400–5–400 K; ● = 4th hysteresis loop: 400–5–400 K.

cooling from room temperature to 5 K leads to a “normal” steady decrease of $\chi_{\text{M}}T$ to a low-temperature plateau at around 1.5 $\text{cm}^3\text{K mol}^{-1}$, on annealing of this sample $\chi_{\text{M}}T$ decreases between 220 and 270 K, whereas only on further warming is a spin-crossover behavior like that observed for $[\text{Fe}(\mathbf{1c})_2](\text{OTf})_2$ (Figure 6) found. $\chi_{\text{M}}T$ reaches a value of 2.4 $\text{cm}^3\text{K mol}^{-1}$ at 400 K, and on recooling—as in the case of $[\text{Fe}(\mathbf{1c})_2](\text{OTf})_2$ —a hysteresis is observed, which on re-annealing features a minimum again (Figure 8). With every heating–cooling cycle the minimum at 220–270 K loses depth but is always clearly visible. Since thermodynamically it is not plausible that the partitioning of the low-spin state becomes higher at any stage of the temperature range on warming, the minimum should be associated with a structur-

al phase transition within this temperature range that favors the low-spin state.^[29] Hence, a DSC measurement was carried out, which, however, only showed a maximum at 350 K, which corresponds to the low-spin → high-spin transition. No feature around 250 K was observed. These results concerning the solid-state magnetic behavior of [Fe(**3a**)₂](OTf)₂ reveal several important aspects: The hysteresis and high-spin trapping observed for [Fe(**1c**)₂](OTf)₂ are not due to the OTf residue but apparently a property inherent to the btp framework. Secondly, it becomes clear that for the solid-state samples the substitution pattern of the btp ligands sensitively influences the magnetic properties of the resulting complexes, but the behavior is not predictable, since solid-state packing interferes and mainly contributes to the overall effects observed. To eradicate solid-state effects and unravel their intrinsic magnetic properties, the complexes [Fe(btp)₂](OTf)₂ (btp = **1c**, **1b**, **3a**) were also investigated in solution by using the Evans method, which indeed indicated a clear trend: dissolved in acetonitrile at room temperature [Fe(**1c**)₂](OTf)₂ again adopts a low-spin configuration as in the solid state, and—also consistently—a high-spin contribution was found for [Fe(**1b**)₂](OTf)₂, albeit to a much smaller extent than that in the solid state (1.6 μ_B; such differences between the solid-state and solution behavior are rather common^[25]). The high-spin partitioning was even more pronounced in the case of [Fe(**3a**)₂](OTf)₂ (3.4 μ_B), and therefore the ligand-field splitting decreases with increasing donor character of the btp ligands. This should also be reflected in the redox properties of btp complexes (through the positioning of the t_{2g} orbital set), which was investigated using Ru²⁺ instead of Fe²⁺ as the central atom, since the Ru complexes persist as 1:2 complexes in solution, in contrast to their highly dynamic Fe analogues (vide infra).

Redox properties: To gain a better understanding of the influence that residues bound to the btp scaffold have on the electronic properties of coordinated metal centers, cyclic voltammetry measurements with various [Ru(btp)₂](PF₆)₂ complexes were performed. Cyclic voltammograms of [Ru(**3a**)₂](PF₆)₂, [Ru(**1b**)₂](PF₆)₂, [Ru(**3b**)₂](PF₆)₂, and [Ru(**3c**)₂](PF₆)₂ display qualitatively similar redox behavior yet the characteristic one-electron oxidation waves are strongly shifted depending on the ligand attached (Figure 9).

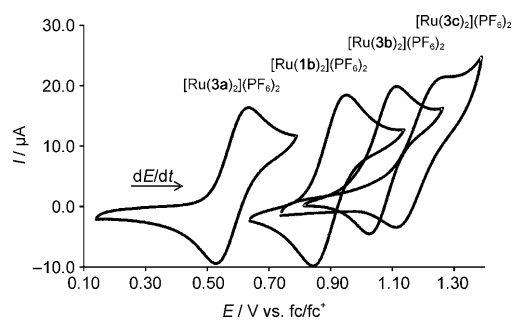


Figure 9. Cyclic voltammetry of various Ru-(btp)₂ complexes (1 mM, 200 mV s⁻¹, 0.1 M (nBu)₄NPF₆, PhCN) versus the ferrocene/ferrocenium (fc/fc⁺) couple.

The measured oxidation potentials clearly correlate with the electron-donating ability of the substituent in the 4-position attached to the central pyridine moiety of the btp ligand, which leads to lower oxidation potentials when more strongly donating substituents are incorporated.^[30] For example, the Ru²⁺ center in [Ru(**3a**)₂](PF₆)₂ is oxidized to Ru³⁺ at a potential of 0.58 V. This is significantly lower than the potentials required to oxidize the three other complexes and is consistent with the strongly electron-donating properties of the pyrrolidyl substituent in ligand **3a**. On the other hand, by attaching an electron-withdrawing ester substituent as in [Ru(**3c**)₂](PF₆)₂ the metal center is oxidized at a significantly higher potential of 1.19 V. Remarkably, simple variation of one substituent attached to the central pyridine moiety of the btp scaffold enables shifting of the Ru²⁺ oxidation potential over a range exceeding 0.6 V (Table 1).

Table 1. Half-wave potentials and peak potential differences of investigated [Ru(btp)₂]²⁺ complexes versus the ferrocene/ferrocenium (fc/fc⁺) couple determined from cyclic voltammetry (Figure 9).

Complex	$E_{1/2}$ [V]	ΔE_p [mV]
[Ru(3a) ₂](PF ₆) ₂	0.58	102
[Ru(1b) ₂](PF ₆) ₂	0.89	86
[Ru(3b) ₂](PF ₆) ₂	1.06	98
[Ru(3c) ₂](PF ₆) ₂	1.19	152

A more quantitative analysis of the data is possible by involving classical linear free-energy relationships, which correlate chemical-reaction parameters, such as equilibrium constants or rates, with substituent effects (in π-conjugated systems).^[31] When plotting the measured half-wave potentials against Hammett's prominent σ_{para} values of the respective substituents,^[32] a clear linear correlation was found (Figure 10).^[31f,33] This finding illustrates that the electron-donating ability of the central pyridine moiety strongly influences the oxidation potential of the bound metal center and furthermore implies that a predictable fine-tuning of redox

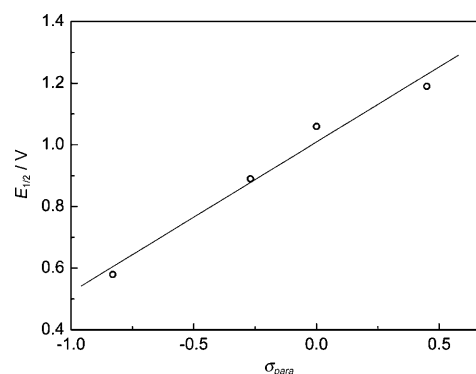


Figure 10. Half-wave potential of the investigated [Ru(btp)₂]²⁺ complexes determined from cyclic voltammetry (Figure 9, Table 1) in relation to the σ_{para} values of their btp substituents R¹ ($\sigma_{para}(-NMe_2) = -0.83$; $\sigma_{para}(-OMe) = -0.27$; $\sigma_{para}(-H) = 0$; $\sigma_{para}(-CO_2Me) = 0.45$).^[32] The line shows the linear fit ($R = 0.98836$).

properties by substitution of the btp ligand framework is possible.

By considering that pyridine-based ligands with two flanking imido units, namely, bis(imino)pyridines, have proved non-innocent in reductions of their corresponding $[\text{ML}_2]^{2+}$ complexes ($M=\text{Ni, Zn, Fe}$), as indicated by two reversible reduction waves between -1 and -2 V,^[34] we have also investigated the electrochemical reduction of $[\text{Ru}(\text{btp})_2](\text{PF}_6)_2$ complexes. In the case of $[\text{Ru}(\mathbf{3b})_2](\text{PF}_6)_2$ at -1.0 V a reductive current starts to flow and increases until -2.0 V (with a shoulder at -1.5 V) but the corresponding process is not reversible. However, $[\text{Ru}(\mathbf{3c})_2](\text{PF}_6)_2$ exhibited two reversible reduction waves at 1.06 and 1.27 V, even though $\mathbf{3c}$ itself cannot be reduced reproducibly. The seemingly contradictory findings stimulate efforts to carry out the two reduction steps chemically to isolate and characterize the resulting product(s) in the future.

Complex stability: Although the magnetic and electronic properties of the various btp complexes are clearly strongly influenced by substitution, we investigated the influence of the differently substituted btp ligands on the stability of their complexes. For this purpose, isothermal titration calorimetry (ITC) measurements were performed to monitor the formation of Fe^{2+} complexes from $[\text{Fe}(\text{OTf})_2(\text{CH}_3\text{CN})_2]$ on treatment with two btp ligand series $\mathbf{1a-d}$ and $\mathbf{2a-c}$. Fe^{2+} instead of Ru^{2+} was employed to ensure fast ligand-exchange kinetics, which is a prerequisite for reliable ITC measurements. Although ITC has received rather little attention in the field of coordination chemistry,^[35] it can provide detailed insight into the thermodynamics of complexation processes and hence the strength of metal–ligand interactions.^[36] ITC measurements were carried out by titrating small aliquots of $[\text{Fe}(\text{OTf})_2(\text{CH}_3\text{CN})_2]$ into a solution of the respective btp ligand in acetonitrile, and after averaging three independent titration experiments on each ligand and correction for the heat of dilution (Figure 17 in the Supporting Information), thermodynamic parameters describing the complexation equilibria could be extracted (Table 2).

Quantitative analysis of the data shows cumulative stability constants (β) in the order of 10^6 – 10^8 M^{-2} for solutions of the $[\text{Fe}(\text{btp})_2](\text{OTf})_2$ complexes in acetonitrile. Although the

stability constants are derived from fitting the data, the corresponding complexation enthalpies can be obtained directly from the measurements and are hence associated with a very small error. Therefore, the complexation enthalpies have been used to compare the substituent effects on the thermodynamics of complex formation. The measured overall complexation enthalpies range from -13 to $-18 \text{ kcal mol}^{-1}$ depending on the ligand and its substitution pattern. Donor substitution—not only at the central pyridine but also at the terminal phenyl moieties—clearly increases the exothermicity of complexation. Interestingly, series $\mathbf{1a-c}$ spans a much wider range ($\Delta\Delta H=5.0 \text{ kcal mol}^{-1}$) than series $\mathbf{2a-c}$ ($\Delta\Delta H=1.5 \text{ kcal mol}^{-1}$), which illustrates the stronger influence of the terminal substituents R^2/R^3 in the ether-substituted series $\mathbf{1a-c}$. Given a stronger variation of the R^1 substituents, an even more pronounced alteration of the complexation thermodynamics can be anticipated. Interestingly, $\mathbf{1c}$ shows a lower absolute enthalpy of complexation than $\mathbf{2c}$.

In both ligand series, the measured enthalpies of complexation can be correlated to Hammett's σ_{para} values (Figure 11). The observed linear correlation is rather re-

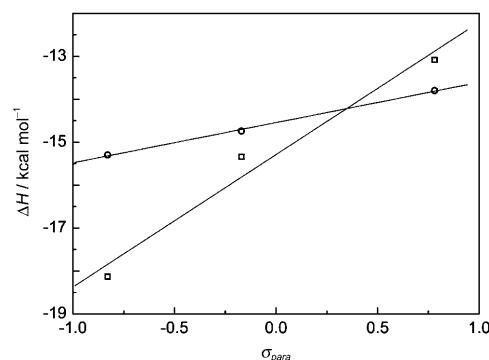


Figure 11. Complexation enthalpies for the formation of $[\text{Fe}(\text{btp})_2](\text{OTf})_2$ complexes of various btp ligands in CH_3CN at 25°C (Table 2) as a function of the σ_{para} values of their substituents R^2 and R^3 .^[32] Squares: $\mathbf{1a-c}$ ($\text{R}^1=\text{OTg}$), circles: $\mathbf{2a-c}$ ($\text{R}^1=\text{COOTg}$). The lines show the fit of the data (circles: $R=0.98656$; squares: $R=0.99913$).

markable since the terminal substituents are not in true resonance with the coordinating N atoms of the triazole moieties. This finding points to the possibility of charge delocalization across the triazole ring system.^[37] In addition, the observed linearity indicates that within the investigated series the entropic contribution to complexation does not vary significantly and hence differences in complexation ability most likely are enthalpic in origin.

Clearly, the ITC results are in line with the CV measurements showing a correlation between binding enthalpies and redox potentials, both of which primarily depend on the donating/accepting properties of the ligands by considering the respective metal center (Fe or Ru). However, the ITC results, which indicate a strengthening of the Fe–btp interaction with increasing electron density within the btp frame-

Table 2. Cumulative stability constants and corresponding enthalpies for formation of $[\text{Fe}(\text{btp})_2](\text{OTf})_2$ complexes in CH_3CN at 25°C measured by ITC (average of three independent measurements) starting from an excess amount of btp ligand ($\approx 0.125 \text{ mM}$) and subsequent $[\text{Fe}(\text{OTf})_2(\text{CH}_3\text{CN})_2]$ addition (55 steps of $1 \mu\text{L}$ each of a $\approx 3.125 \text{ mM}$ solution).

btp	$\text{Fe}^{2+} + 2(\text{btp}) \rightarrow [\text{Fe}(\text{btp})_2]^{2+}$	
	$\beta [\text{M}^{-2}]$	$\Delta H [\text{kcal mol}^{-1}]$
1a	$\approx 10^8$	-18.13 ± 0.14
1b	$\approx 10^8$	-15.34 ± 0.12
1c	$\approx 10^7$	-13.08 ± 0.13
1d	$\approx 10^7$	-14.05 ± 0.14
2a	$\approx 10^7$	-15.30 ± 0.07
2b	$\approx 10^7$	-14.74 ± 0.09
2c	$\approx 10^6$	-13.82 ± 0.13

work, seem to contradict those of the magnetic measurements. A strong interaction is usually associated with a strong ligand field and thus with a large $t_{2g}-e_g$ separation, which should favor low-spin states. However, while the binding enthalpy of **1b** (absolute value) is higher than the one of **1c**, still the partitioning of the low-spin state decreases on going from **1c** to **1b**. This can be explained in a simplistic way assuming that the binding enthalpies measured are mainly due to Fe–N σ interactions and will increase with increasing “N base strength”, that is, with increasing electron density. However, the substituents also sensitively influence the energetic positions of the ligand π and π^* orbitals and thus their interaction with the metal t_{2g} and e_g orbitals, which also determines the $t_{2g}-e_g$ separation. For phenanthroline derivatives this has already led to counterintuitive ligand-field splittings in the past.^[38] Apparently, also in our case, the substituents influence the contribution of the π interactions to the $t_{2g}-e_g$ separation more strongly and in an opposite direction than the contribution of the σ interactions, which, however, mainly determine the binding enthalpies. Note that NO₂ groups will reduce the σ -donor capacity, while the π -accepting ability is enhanced.

To gain further insight into the relative importance of terminal and central substituents on complexation thermodynamics, ITC experiments were also performed with derivative **1d**, which carries a donor on one phenyl terminus while carrying an acceptor on the other terminus. Within the ether-substituted series (**1a–d**), **1d** does not display an exact intermediate complexation enthalpy but is rather similar to **1c**, which suggests that acceptor substitution is dominating the ligand behavior.

Complexation equilibria: From the ITC curves showing pronounced exotherms of equal intensity until half an equivalent of $[\text{Fe}(\text{OTf})_2(\text{CH}_3\text{CN})_2]$ has been added (Figure 18 in the Supporting Information), it is apparent that 1:2 complexes, that is, $[\text{Fe}(\text{btp})_2]^{2+}$, are formed. Clearly, considerable energy is released upon exchange of the weakly coordinating acetonitrile/triflate ligands by the tridentate btp ligand framework. This observation is further supported by the isolation of $[\text{Fe}(\mathbf{1c})_2](\text{OTf})_2$ ^[9] from one such reaction, and subsequent UV/Vis titrations of **1b** with $[\text{Fe}(\text{OTf})_2(\text{CH}_3\text{CN})_2]$ (Figure 12) also corroborated these findings.

Addition of the Fe²⁺ ions is indicated by the evolution of three different bands: 1) the hypsochromically shifted ligand $\pi \rightarrow \pi^*$ absorption ($\lambda_{\text{max}} = 293$ nm), 2) the $\pi \rightarrow \pi^*$ absorption associated with the *syn, syn* conformation of the ligands ($\lambda_{\text{max}} = 345$ nm), and 3) the MLCT transition ($\lambda_{\text{max}} = 430$ nm).^[39] Note that the UV/Vis spectra of various $[\text{Ru}(\text{btp})_2]^{2+}$ complexes^[13] show pronounced changes in the energy and intensity of the MLCT transition, again pointing to significant electronic modulation of the complexes by ligand substitution, although in this case no simple linear correlation was found (Figure 15 in the Supporting Information). Relative to the analogous tpy-based Fe complexes, the MLCT transition in the btp complexes is hypsochromically shifted by approximately 100 nm. The presence of several

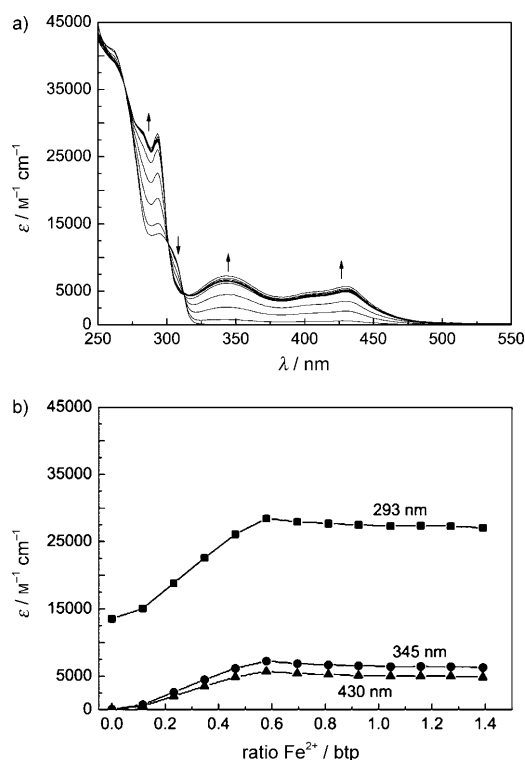


Figure 12. a) UV/Vis titration of **1b** (3.51×10^{-5} M) with $[\text{Fe}(\text{OTf})_2(\text{MeCN})_2]$ (0–1.4 equiv) in acetonitrile at 25°C. b) Molar extinction coefficient in relation to the Fe²⁺/btp ratio for 293 (squares), 345 (circles), and 430 nm (triangles).

isosbestic points ($\lambda = 269, 301, 312$ nm) indicates a unimolecular process and thus the presence of only two absorbing species, further supported by a more rigorous analysis using extinction difference diagrams^[40] (Figure 14 in the Supporting Information). The absorption arising from the formed complex ($\lambda_{\text{max}} = 293, 345, 430$ nm) continues to increase upon addition of $[\text{Fe}(\text{OTf})_2(\text{CH}_3\text{CN})_2]$ until a 1:2 ratio of Fe/btp has been reached (Figure 12b), as expected on the basis of the ITC measurements. Furthermore, the 1:2 stoichiometry of the formed complex was verified by a Job plot^[41] (Figure 16 in the Supporting Information), and the shape of the actual Job curve, which is known to depend on the complex stability in a characteristic manner,^[41c] was in excellent agreement with the stability constant of 10^8 M^{-2} derived from the ITC measurements.

Complexation dynamics: As pointed out, $[\text{Fe}(\mathbf{1c})_2](\text{OTf})_2$ adopts a low-spin configuration both in the solid state and in solution (vide supra). Consistently, on dissolution of $[\text{Fe}(\mathbf{1c})_2](\text{OTf})_2$ in CD₃CN the ¹H NMR spectrum shows one sharp signal set for the protons associated with the bound btp ligand, with all resonances being shifted (to different extents) downfield relative to free **1c**. Nevertheless, more thorough NMR spectroscopic titration experiments to complement the UV/Vis experiments were carried out with ligand **1b** (Figure 13a–e): $[\text{Fe}(\mathbf{1b})_2](\text{OTf})_2$ dissolved in CD₃CN also

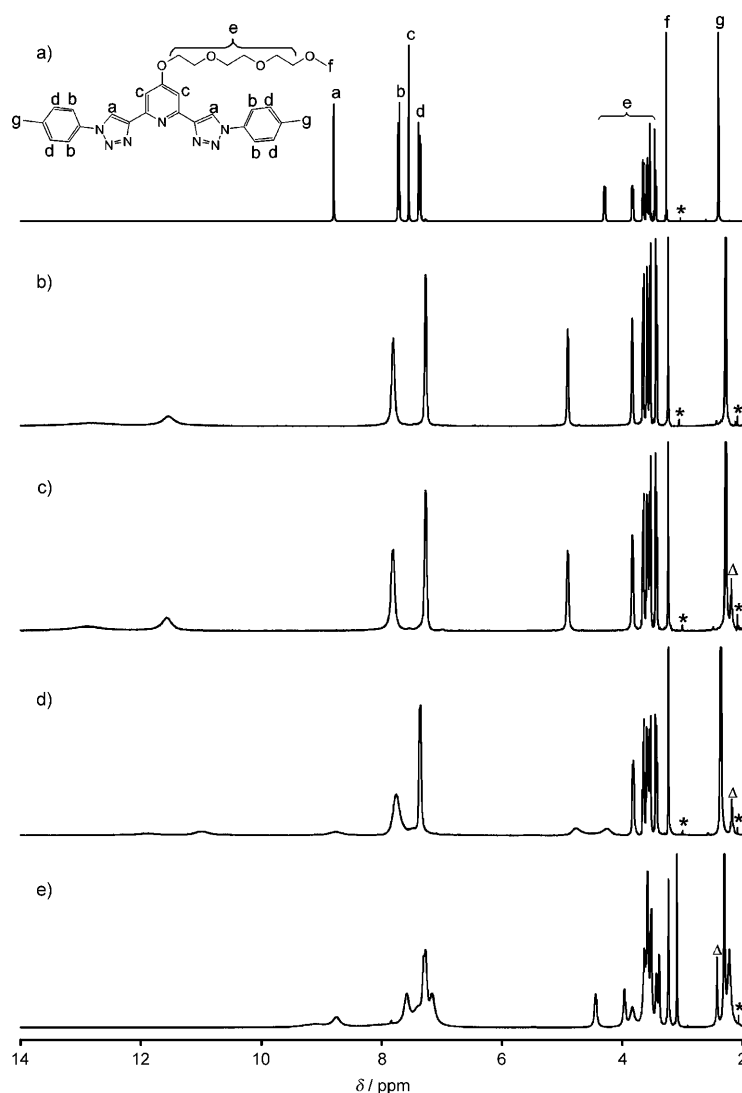


Figure 13. ^1H NMR spectra of a) **1b**, b) $[\text{Fe}(\mathbf{1b})_2](\text{OTf})_2$, c) $2\mathbf{1b} + [\text{Fe}(\text{OTf})_2(\text{CH}_3\text{CN})_2]$, d) $[\text{Fe}(\mathbf{1b})_2](\text{OTf})_2 + 2\mathbf{1b}$ at RT, and e) $[\text{Fe}(\mathbf{1b})_2](\text{OTf})_2 + 2\mathbf{1b}$ at -30°C measured in CD_3CN . For a more informative representation, signals f and g are not shown in their full height. Signals marked with * can be attributed to impurities, those marked with Δ belong to CH_3CN .

primarily exhibits low-spin character (vide supra) and beyond that offers enhanced solubility relative to $[\text{Fe}(\mathbf{1c})_2](\text{OTf})_2$.

Similarly as for $[\text{Fe}(\mathbf{1c})_2](\text{OTf})_2$, there is no difference between the spectra of the isolated complex $[\text{Fe}(\mathbf{1b})_2](\text{OTf})_2$ (Figure 13b) and the 1:2 mixture of $[\text{Fe}(\text{OTf})_2(\text{CH}_3\text{CN})_2]$ and ligand **1b** (Figure 13c). Upon addition of two further equivalents of ligand **1b** to a 1:2 sample, giving rise to a Fe/btp ratio of 1:4, mainly the 1:2 complex and free ligand would be expected to be present in solution, and it is interesting to note that performing such an NMR spectroscopic experiment with the tpy ligand indeed leads to two sets of signals at room temperature: one for free tpy and one for $[\text{Fe}(\text{tpy})_2](\text{OTf})_2$ in a 1:1 ratio. Surprisingly, no second signal set appeared within the spectrum of a $[\text{Fe}(\text{OTf})_2(\text{CH}_3\text{CN})_2]/$

4 **1b** sample, and instead only a broadening of all signals belonging to the btp framework was observed (Figure 13d). This finding could in principle be rationalized by a rapid ligand exchange. To investigate the ligand-exchange dynamics the sample was cooled to 243 K,^[42] which led to severe changes in the spectrum (Figure 13e). Several new resonances appear in the aromatic as well as aliphatic regions, which suggests that now the signals of both the free and the coordinated btp molecules can be detected due to the decelerated ligand exchange. Although most signals could not be assigned unambiguously,^[43] the observed splitting of the signal associated with the terminal methyl group (signal g in Figure 13) indicates that indeed complex and ligand coexist in an approximate 1:2 ratio, as expected by the given stoichiometry (note that the spectrum of the free btp ligand does not undergo any changes upon cooling).

The results of the NMR spectroscopic investigations clearly show that ligand-exchange dynamics for the btp/ Fe^{II} system in acetonitrile at room temperature are fast on the NMR spectroscopic timescale, which represents a marked difference to the corresponding tpy chemistry. Consequently, addition of two equivalents of tpy to a solution of $[\text{Fe}(\mathbf{1b})_2](\text{OTf})_2$ in CD_3CN leads to two signal sets: one for $[\text{Fe}(\text{tpy})_2](\text{OTf})_2$ and one for uncomplexed **1b**. In addition to a fast ligand exchange, further equilibria in solution are possibly involved, considering that ESI/MS measurements performed with $[\text{Fe}(\mathbf{1b})_2](\text{OTf})_2$ dissolved in CH_3CN showed (amongst others) peaks for $[\text{Fe}(\mathbf{1b})_x]^{2+}$ ($x=2-6$) and $[\text{Fe}(\mathbf{1b})_2(\text{OTf})]^+$ (Figure 42 in the Supporting Information).^[44] This naturally raises the question of the role of acetonitrile in these dynamics, especially considering that it is needed for the occupation of the free coordination sites generated. Indeed, performing the same NMR spectroscopic experiments in CD_2Cl_2 revealed that the ability of the solvent to coordinate to the metal center is crucial for the establishment of the equilibrium described above: On dissolution of $[\text{Fe}(\mathbf{1b})_2](\text{OTf})_2$ together with **1b** in CD_2Cl_2 two very sharp sets of signals are observed, one of which is identical to the spectrum displayed by free **1b**. Hence, it is possible to influence the complex stability and the possibility of ligand exchange by the solvent, which may be utilized for the design of more complex structures in the future. Furthermore it should be pointed out that the corresponding Ru complexes are also stable in acetonitrile in which no ligand exchange could be detected, a prerequisite for reasonable CV data (vide supra).

Conclusion

By exploiting the synthetic versatility of click chemistry, btp ligands with a wide range of substitution patterns were prepared in a modular fashion. The redox properties as well as the thermodynamic stability of their resulting transition-metal complexes, in particular Fe^{II} and Ru^{II} , display an excellent correlation to the electronic properties of the ligands. The observed linear relationship with Hammett's substituent

constants enables the precise fine-tuning of btp ligands to yield btp complexes with predictable electronic properties. For example, oxidation potentials of $[\text{Ru}(\text{btp})_2]^{2+}$ complexes can predictably be tuned within a range of 610 mV by simple ligand substitution. The magnetic behavior of the iron complexes in solution is sensitively and consistently influenced by the substitution pattern, too, while the magnetic investigation of solid samples revealed very interesting features such as hystereses, high-spin locking through tempering, and “low-spin minima”, the origin of which remains to be understood.

When comparing the btp ligand scaffold with established tridentate nitrogen-based ligands, in particular tpy, btp ligands maintain considerable complex stabilities while offering the advantage of much faster ligand-exchange dynamics. This should lead to improved properties in supramolecular polymeric materials,^[1b,45] as the self-healing is accelerated.

Acknowledgements

The authors thank C. Knispel, P. Neubauer, and Dr. B. Ziemer (HU Berlin) for carrying out the single-crystal X-ray structure analyses and Dr. H. Hennig and Prof. N. P. Ernsting for their help with using the isothermal titration calorimeter. Generous support by ERA Chemistry (Project “SurConFold”), the German Research Foundation (DFG via SFB 765), the Fonds der Chemischen Industrie, the Bundesministerium für Bildung, Wissenschaft, Forschung und Technologie, and the Dr. Otto Röhm Gedächtnisstiftung is gratefully acknowledged. Wacker Chemie AG, BASF AG, Bayer Industry Services, and Sasol Germany are thanked for generous donations of chemicals.

- [1] Original work: a) G. T. Morgan, F. H. Burstall, *J. Chem. Soc.* **1932**, 20–30. A comprehensive treatment is given in: b) U. S. Schubert, H. Hofmeier, G. R. Newkome in *Modern Terpyridine Chemistry*, Wiley-VCH, Weinheim, **2006**.
- [2] Original work: a) H. Nishiyama, H. Sakaguchi, T. Nakamura, M. Horihata, M. Kondo, K. Itoh, *Organometallics* **1989**, *8*, 846–848. For a review, see: b) G. Desimoni, G. Faita, P. Quadrelli, *Chem. Rev.* **2003**, *103*, 3119–3154.
- [3] For a review, see: M. A. Halcrow, *Coord. Chem. Rev.* **2005**, *249*, 2880–2908.
- [4] For a review, see: V. Balzani, A. Juris, M. Venturi, S. Campagna, S. Serroni, *Chem. Rev.* **1996**, *96*, 759–833.
- [5] Reviews are given in: a) O. Sato, J. Tao, Y.-Z. Zhang, *Angew. Chem.* **2007**, *119*, 2200–2236; *Angew. Chem. Int. Ed.* **2007**, *46*, 2152–2187; b) O. Kahn in *Molecular Magnetism*, VCH, Weinheim, **1993**.
- [6] Reviews are given in: a) A. K. Ghosh, P. Mathivanan, J. Cappiello, *Tetrahedron: Asymmetry* **1998**, *9*, 1–45; b) J. S. Johnson, D. A. Evans, *Acc. Chem. Res.* **2000**, *33*, 325–335.
- [7] The term “click chemistry” usually refers to the Cu-catalyzed 1,3-dipolar cycloaddition reaction, pioneered by: a) V. V. Rostovtsev, L. G. Green, V. V. Fokin, K. B. Sharpless, *Angew. Chem.* **2002**, *114*, 2708–2711; *Angew. Chem. Int. Ed.* **2002**, *41*, 2596–2599 and b) C. W. Tornøe, C. Christensen, M. Meldal, *J. Org. Chem.* **2002**, *67*, 3057–3064. For a recent and comprehensive review, see: c) M. Meldal, C. W. Tornøe, *Chem. Rev.* **2008**, *108*, 2952–3015.
- [8] The general concept of click chemistry has been introduced in: H. C. Kolb, M. G. Finn, K. B. Sharpless, *Angew. Chem.* **2001**, *113*, 2056–2075; *Angew. Chem. Int. Ed.* **2001**, *40*, 2004–2021.
- [9] a) R. M. Meudtner, M. Ostermeier, R. Goddard, C. Limberg, S. Hecht, *Chem. Eur. J.* **2007**, *13*, 9834–9840; b) M.-A. Berlin, M. Ostermeier, R. M. Meudtner, C. Limberg, S. Hecht, *Polym. Prepr. Am. Chem. Soc. Div. Polym. Chem.* **2009**, *50*, 261.
- [10] Responsive “clickamers”: a) R. M. Meudtner, S. Hecht, *Angew. Chem.* **2008**, *120*, 5004–5008; *Angew. Chem. Int. Ed.* **2008**, *47*, 4926–4930. Helically folding polymers and their gels: b) R. M. Meudtner, S. Hecht, *Macromol. Rapid Commun.* **2008**, *29*, 347–351. Switchable 2D self-assembly at surfaces: c) L. Piot, R. M. Meudtner, T. El Mahlah, S. Hecht, P. Samori, *Chem. Eur. J.* **2009**, *15*, 4788–4792.
- [11] Related work has appeared in: a) Y. Li, J. C. Huffman, A. H. Flood, *Chem. Commun.* **2007**, 2692–2694; b) J. T. Fletcher, B. J. Bumgarner, N. D. Engels, D. A. Skoglund, *Organometallics* **2008**, *27*, 5430–5433; c) B. Schulze, C. Friebe, M. D. Hager, A. Winter, R. Hoogenboom, H. Görls, U. S. Schubert, *Dalton Trans.* **2009**, 787–794.
- [12] E. C. Constable, G. Baum, E. Bill, R. Dyson, R. van Eldik, D. Fenske, S. Kaderli, D. Morris, A. Neubrand, M. Neuberger, D. R. Smith, K. Wieghardt, M. Zehnder, A. D. Zuberbühler, *Chem. Eur. J.* **1999**, *5*, 498–508.
- [13] See the Supporting Information.
- [14] a) B. L. Small, M. Brookhart, A. M. A. Bennett, *J. Am. Chem. Soc.* **1998**, *120*, 4049–4050; b) G. J. P. Britovsek, V. C. Gibson, B. S. Kimberley, P. J. Maddox, S. J. McTavish, G. A. Solan, A. J. P. Whitea, D. J. Williams, *Chem. Commun.* **1998**, 849–850; c) Q. Knijnenburg, A. D. Horton, H. van der Heijden, T. M. Kooistra, D. G. H. Heterscheid, J. M. M. Smits, B. de Bruin, P. H. M. Budzelaar, A. W. Gal, *J. Mol. Catal. A* **2005**, *232*, 151–159.
- [15] J.-P. Sauvage, J.-P. Collin, J.-C. Chambron, S. Guillerez, C. Coudret, V. Balzani, F. Barigelletti, L. De Cola, L. Flamigni, *Chem. Rev.* **1994**, *94*, 993–1019.
- [16] a) T. Norrby, A. Börje, B. Åkermark, L. Hammarström, J. Alsins, K. Lashgari, R. Norrestam, J. Mårtensson, G. Stenhagen, *Inorg. Chem.* **1997**, *36*, 5850–5858; b) E. Alessio, *Chem. Rev.* **2004**, *104*, 4203–4242.
- [17] CCDC-759265 (**3a**), -759266 (**3b**), -759267 ($[\text{Ru}(\mathbf{3b})_2](\text{PF}_6)_2$), -759268 ($[\text{Ru}(\mathbf{1b})_2](\text{PF}_6)_2$), -759269 ($[\text{Zn}(\mathbf{1a})(\text{Br})_2]$), -759270 (**3c**), -759271 ($[\text{Ru}(\mathbf{3c})_2](\text{PF}_6)_2$), -759272 ($[\text{Ru}(\mathbf{3a})](\text{PF}_6)_2$), and 759273 ($[\text{Ru}(\mathbf{3c})(\text{dmsO})\text{Cl}_2]$) contain the supplementary crystallographic data for this paper. These data can be obtained free of charge from The Cambridge Crystallographic Data Centre via www.ccdc.cam.ac.uk/data_request/cif.
- [18] a) A. Knödler, W. Kaim, *Z. Anorg. Allg. Chem.* **2005**, *631*, 491–495; b) R. Ziessel, V. Grosshenny, M. Hissler, C. Stroh, *Inorg. Chem.* **2004**, *43*, 4262–4271.
- [19] A. W. Addison, T. N. Rao, J. Reedijk, G. C. Verschoor, *J. Chem. Soc. Dalton Trans.* **1984**, 1349–1356.
- [20] a) D. E. C. Corbridge, E. G. Cox, *J. Chem. Soc.* **1956**, 594–603; b) F. W. B. Einstein, B. R. Penfold, *Acta Crystallogr.* **1966**, *20*, 924–926; c) M. Vlasse, T. Rojo, D. Beltran-Porter, *Acta Crystallogr. Sect. C* **1983**, *39*, 560–563.
- [21] C. Janiak, *J. Chem. Soc. Dalton Trans.* **2000**, 3885–3896.
- [22] The distances between the carbon atoms binding the hydrogen atoms, which are considered to be responsible for the hydrogen bonds, and the halogen atoms are comparable to the sum of the van der Waals (vdW) radii of the halogen and carbon atoms: $\Sigma[r_{\text{vdW}}(\text{Cl})]$, $r_{\text{vdW}}(\text{C})=3.5 \text{ \AA}$, distances Cl–C found in the crystal structure of $[\text{Ru}(\mathbf{3c})\text{Cl}_2(\text{dmsO})]=3.5 \text{ \AA}$; $\Sigma[r_{\text{vdW}}(\text{Br})]$, $r_{\text{vdW}}(\text{C})=3.6 \text{ \AA}$, distances Br–C found in the crystal structure of $[\text{Zn}(\mathbf{1a})\text{Br}_2]=3.6\text{--}3.7 \text{ \AA}$.
- [23] V. Grosshenny, R. J. Ziessel, *Organomet. Chem.* **1993**, *22*, C19–C22.
- [24] a) A similar strategy has been applied before for the synthesis of $[\text{RuL}_2]^{2+}$ complexes with **L** representing—for instance—tripodal phosphane ligands. b) Compare also: L. F. Rhodes, C. Sorato, L. M. Venanzi, F. Bachechi, *Inorg. Chem.* **1988**, *27*, 604–610.
- [25] P. Gütllich, A. Hauser, H. Spiering, *Angew. Chem.* **1994**, *106*, 2109–2141; *Angew. Chem. Int. Ed. Engl.* **1994**, *33*, 2024–2054.
- [26] T. Buchen, P. Gütllich, K. H. Sugiyarto, H. A. Goodwin, *Chem. Eur. J.* **1996**, *2*, 1134–1138.
- [27] a) J. M. Holland, J. A. McAllister, Z. Lu, C. A. Kilner, M. Thornton-Pett, M. A. Halcrow, *Chem. Commun.* **2001**, 577–578; b) J. M. Holland, J. A. McAllister, C. A. Kilner, M. Thornton-Pett, A. J. Bridgeman, M. A. Halcrow, *J. Chem. Soc. Dalton Trans.* **2002**, 548–554; c) J. Elhaik, D. J. Evans, C. A. Kilner, M. A. Halcrow, *Dalton Trans.*

- 2005, 1693–1700; d) J. Elhaik, C. A. Kilner, M. A. Halcrow, *Dalton Trans.* **2006**, 823–830.
- [28] The isomer shift of $[\text{Fe}(\mathbf{1c}_2)(\text{OTf})_2]$ with $\delta = 0.36 \text{ mm s}^{-1}$ is comparable to that of $[\text{Fe}(\text{bpy})_3](\text{ClO}_4)_2$ ($\delta = 0.325 \text{ mm s}^{-1}$; R. L. Collins, R. Pettit, W. A. Baker, Jr., *J. Inorg. Nucl. Chem.* **1966**, 28, 1001–1010). $[\text{Fe}(\mathbf{L}_2)(\text{PF}_6)_2$ ($\mathbf{L} = 2,6\text{-bis}[1\text{-}(4\text{-methoxyphenylimino)ethyl]pyridine}$; $\delta = 0.235(8) \text{ mm s}^{-1}$ (xa)) and $[\text{Fe}(\text{tpy})_2](\text{ClO}_4)_2$ ($\delta = 0.238 \text{ mm s}^{-1}$; L. M. Epstein, *J. Chem. Phys.* **1964**, 40, 435–439) show significantly lower isomer shifts than those of $[\text{Fe}(\mathbf{1c}_2)(\text{OTf})_2]$ or $[\text{Fe}(\text{bpy})_3](\text{ClO}_4)_2$, which indicates a greater charge delocalization from the metal t_{2g} orbitals into the ligand π^* orbitals through π back-donation.
- [29] When one phase at low temperature prefers the high-spin state and another at high temperature prefers the low-spin state, a traverse through a minimum can be observed; compare S. Hayami, Y. Shigeyoshi, M. Akita, K. Inoue, K. Kato, K. Osaka, M. Takata, R. Kawajiri, T. Mitani, Y. Maeda, *Angew. Chem.* **2005**, 117, 4977–4981; *Angew. Chem. Int. Ed.* **2005**, 44, 4899–4903.
- [30] Trying to fit the btp ligands into the electrochemical series developed by A. B. P. Lever et al. (A. B. P. Lever, *Inorg. Chem.* **1990**, 29, 1271–1285) requires the treatment of the $[\text{Ru}(\text{btp})_2]^{2+}$ compounds as $[\text{Ru}(\mathbf{L})_6]^{2+}$ -type complexes. Corresponding averaging over six positions leads to values of $E_L = 0.21$ (**3a**), 0.26 (**1b**), 0.29 (**3b**), and 0.31 (**3c**).
- [31] a) L. P. Hammett, *J. Am. Chem. Soc.* **1937**, 59, 96–103; For a review, see: b) C. Hansch, A. Leo, R. W. Taft, *Chem. Rev.* **1991**, 91, 165–195; c) H. H. Jaffé, *Chem. Rev.* **1953**, 53, 191–261. Application in coordination chemistry: d) S. Dutta, B. R. Jagirdar, M. Nethaji, *Inorg. Chem.* **2008**, 47, 548–557; e) O. Zekri, E. A. Hillard, S. Top, A. Vesières, P. Pigeon, M.-A. Plamont, M. Huché, S. Boutamine, M. J. McGlinchey, H. Müller-Bunz, G. Jaouen, *Dalton Trans.* **2009**, 4318–4326; f) M. Sjödin, J. Gätjens, L. C. Tabares, P. Thuéry, V. L. Pecoraro, S. Un, *Inorg. Chem.* **2008**, 47, 2897–2908; g) N. J. De Yonker, N. A. Foley, T. R. Cundari, T. B. Gunnoe, J. L. Petersen, *Organometallics* **2007**, 26, 6604–6611; h) M. Gasperini, F. Ragaini, S. Ceni, *Organometallics* **2002**, 21, 2950–2957; i) J. Chambers, B. Eaves, D. Parker, R. Claxton, P. S. Ray, S. J. Slattery, *Inorg. Chim. Acta* **2006**, 359, 2400–2406.
- [32] C. Hansch, A. Leo, S. H. Unger, K. H. Kim, D. Nikaitani, E. J. Lien, *J. Med. Chem.* **1973**, 16, 1207–1216.
- [33] Even though the complex derived from ligand **1b** carries terminal methyl groups instead of iodine substituents, it nicely matches the linear fit, thus illustrating the dominant role of the central pyridine moiety (vide infra).
- [34] a) B. de Bruin, E. Bill, E. Bothe, T. Weyhermüller, K. Wieghardt, *Inorg. Chem.* **2000**, 39, 2936–2947; b) P. H. M. Budzelaar, B. de Bruin, A. W. Gal, K. Wieghardt, J. H. van Lenthe, *Inorg. Chem.* **2001**, 40, 4649–4655.
- [35] a) I. Jelesarov, H. R. Bosshard, *J. Mol. Recognit.* **1999**, 12, 3–18; b) E. Freire, O. L. Mayorga, M. Straume, *Anal. Chem.* **1990**, 62, 950A–959A; c) M. J. Blandamer, P. M. Cullis, J. B. F. N. Engberts, *J. Chem. Soc. Faraday Trans.* **1998**, 94, 2261–2267. ITC is commonly used in quantifying interaction energies of biomolecules, for a recent review, see: d) B. Pagano, C. A. Mattia, C. Giancola, *Int. J. Mol. Sci.* **2009**, 10, 2935–2957; e) K. Bouchemal, *Drug Discovery Today* **2008**, 13, 960–972; f) H. Heerklotz, J. Seelig, *Biochim. Biophys. Acta Biomembr.* **2000**, 1508, 69–85; g) V. Ball, C. Maechling, *Int. J. Mol. Sci.* **2009**, 10, 3283–3315; h) A. Brown, *Int. J. Mol. Sci.* **2009**, 10, 3457–3477.
- [36] a) R. Dobrawa, P. Ballester, C. R. Saha-Möller, F. Würthner, *ACS Symp. Ser.* **2006**, 928, 43–62; b) R. Dobrawa, M. Lysetska, P. Ballester, M. Grüne, F. Würthner, *Macromolecules* **2005**, 38, 1315–1325.
- [37] π -Conjugation through 1,4-connected 1,2,3-triazole units has been suggested by the work on triazole-containing main-chain polymers, see: a) D. J. V. C. van Steenis, O. R. P. David, G. P. F. van Strijdonck, J. H. van Maarseveen, J. N. H. Reek, *Chem. Commun.* **2005**, 4333–4335; b) S. Bakbak, P. J. Leech, B. E. Carson, S. Saxena, W. P. King, U. H. F. Bunz, *Macromolecules* **2006**, 39, 6793–6795. Preliminary anisotropic induced current density (AICD) calculations support the notion of π conjugation.
- [38] a) J. Fleisch, P. Gütllich, K. M. Hasselbach, *Inorg. Chem.* **1977**, 16, 1979–1984; b) W. Linert, M. Enamullah, V. Gutmann, R. F. Jameson, *Monatsh. Chem.* **1994**, 125, 661–670.
- [39] For a related assignment of absorption bands in the course of $[\text{Fe}(\text{tpy})_2]^{2+}$ formation, see reference [36a].
- [40] a) H. Mauser, *Z. Naturforsch. B* **1968**, 23, 1021–1025; b) H. Mauser, *Z. Naturforsch. B* **1968**, 23, 1025–1030; c) H. Mauser, H.-J. Niemann, R. Kretschmer, *Z. Naturforsch. B* **1968**, 27, 1349–1353; d) H. Mauser, V. Starrock, H.-J. Niemann, *Z. Naturforsch. B* **1968**, 23, 1354–1359.
- [41] a) P. Job, *Ann. Chim.* **1928**, 9, 113–203; b) C. Y. Huang, *Methods Enzymol.* **1982**, 87, 509–525; c) L. Sommer, M. Langová, *Crit. Rev. Anal. Chem.* **1988**, 19, 225–269.
- [42] Further cooling could not be performed due to the substantial viscosity of the CD_3CN solution.
- [43] The spectrum is complicated by the fact that protons, influenced most by the complexation event absorb at low field. However, the complexation-induced large shifts antagonize the resolution of averaged signals into separate ones (unlike in case of the proton signals within the high-field region), since the increased chemical-shift difference results in a lowered coalescence temperature and hence increased signal widths. Therefore, the differentiation between free and complexed btp is not possible at 243 K.
- [44] Note that ESI/MS spectra of the corresponding Ru complex mainly show the expected peaks for $[\text{Ru}(\mathbf{1b})_2]^{2+}$ (Figure 43 in the Supporting Information).
- [45] a) T. Nakano, Y. Okamoto, *Chem. Rev.* **2001**, 101, 4013–4038; b) J. J. L. M. Cornelissen, A. E. Rowan, R. J. M. Nolte, N. A. J. M. Sommerdijk, *Chem. Rev.* **2001**, 101, 4039–4070.

Received: March 23, 2010

Revised: May 20, 2010

Published online: July 23, 2010